Remote Sensing of Environment 329 (2025) 114906

Contents lists available at ScienceDirect

Remote Sensing of Environment

journal homepage: www.elsevier.com/locate/rse

Using UAV images and deep learning to enhance the mapping of deadwood in boreal forests

Janne Mäyrä [a,*], Topi Tanhuanpää [a,b,c], Anton Kuzmin [b], Einari Heinaro [d], Timo Kumpula [b], Petteri Vihervaara [a]

[a] Finnish Environment Institute (Syke), Latokartanonkaari 11, FI-00790, Helsinki, Finland
[b] Department of Geographical and Historical Studies, University of Eastern Finland, Yliopistonkatu 7, FI-80101 Joensuu, Finland
[c] Department of Forest Sciences, University of Helsinki, Latokartanonkaari 7, FI-00790 Helsinki, Finland
[d] School of Forest Sciences, University of Eastern Finland, Yliopistonkatu 7, FI-80101 Joensuu, Finland

ARTICLE INFO

Keywords:
Boreal forests
Deadwood
Object detection
Unoccupied aerial vehicles

ABSTRACT

Deadwood and decaying wood are the most important components for the biodiversity of boreal forests, and around a quarter of all flora and fauna in Finnish forests depend on them, with third of these species being red-listed. However, there is a severe lack of stand-level deadwood data in Finland, as the operational inventories either focus on the large-scale estimates or omit deadwood altogether. Unoccupied Aerial Vehicles (UAVs) are a cost-effective method for remotely mapping small objects, such as fallen deadwood, over compartment-level areas, as even the most spatially accurate commercial satellites and aerial photography provide 30 cm ground sampling distance, compared to less than 5 cm that is easily achievable with UAVs.

In this study, we utilized YOLOv8 by Ultralytics for detecting and segmenting standing and fallen deadwood instances from RGB UAV imagery. Our study consists of two geographically distinct study areas in Finland, Hiidenportti National Park and Evo. We manually annotated around 13 800 deadwood instances to be used as the training and validation data for the instance segmentation models. These annotations were also compared to field-measured deadwood data from Hiidenportti to assess the extent on how much of the deadwood can even be seen from UAV imagery. We also compared how the models perform on another area than from which its training dataset was from, and whether adding data from another areas to the training dataset improves the performance compared to training only with images from one location.

The best performing model achieved test set mask mAP50 score of 0.682 for Hiidenportti and 0.651 for Sudenpesänkangas datasets. For both areas, including imagery from the another area improved the instance segmentation metrics, whereas using data only from another site to train the models produced significantly worse results. While methods utilizing UAV imagery cannot completely replace traditional field work, they should still be considered as an additional tool for field campaigns.

1. Introduction

Dead and decaying wood are central structural components and key elements of biodiversity in boreal forests. Due to their importance to a significant number of endangered species, they are a widely used surrogate for the ecological quality of forest areas (Juutinen et al., 2006; Lassauce et al., 2011; Stokland et al., 2012). However, large-scale estimates on the amount and quality of deadwood are only available in very low spatial resolution. For example, in Finland the national forest inventory (NFI) only produces deadwood estimates at county level. Although these datasets offer statistically reliable data, they lack the ability of finding the extremes, i.e., intensively managed forests and deadwood hot spots (Jonsson et al., 2016; Puletti et al., 2019). Hence, determining the ecological quality of small forest patches with large-scale deadwood estimates remains rather uncertain with the data at hand.

In forest resource mapping, the remote sensing and close-range sensing-based methods have evolved rapidly during the last decades. High resolution datasets, such as airborne Light Detection and Ranging (LiDAR) have made it possible to reliably capture the vertical forest structure, which has enabled precise estimates of, e.g., timber volume (e.g., Næsset, 2002). For example, in Finland, the compartment-level estimates of forest attributes are estimated using an extensive field-measured training set and area-based LiDAR features (Packalén and

* Corresponding author.
E-mail addresses: janne.mayra@syke.fi (J. Mäyrä), topi.tanhuanpaa@syke.fi (T. Tanhuanpää), anton.kuzmin@uef.fi (A. Kuzmin), einari.heinaro@uef.fi (E. Heinaro), timo.kumpula@uef.fi (T. Kumpula), petteri.vihervaara@syke.fi (P. Vihervaara).

https://doi.org/10.1016/j.rse.2025.114906
Received 28 June 2024; Received in revised form 11 April 2025; Accepted 4 July 2025
Available online 22 July 2025

Maltamo, 2007; Tuominen et al., 2014). Especially in mature forests, the current remote sensing-based technologies enable efficient forest management with limited need for field work at the level of individual forest compartments. However, the current methods only excel in attributes strongly linked with the three-dimensional structure of forest canopy and the lack of compartment-level field work leaves the loosely linked attributes, such as fallen deadwood, to very little attention. As forest management alters the natural processes of deadwood accumulation, the canopy characteristics do not explain the amount and quality of fallen deadwood (e.g., Gibb et al., 2005; Pasher and King, 2009). Hence, there have been several approaches for capturing the fallen deadwood directly from very high-resolution datasets utilizing both airborne LiDAR (Blanchard et al., 2011; Mücke et al., 2013; Polewski et al., 2015; Heinaro et al., 2021) and optical data sets (Inoue et al., 2014; Pirotti et al., 2016; Sylvain et al., 2019; Thiel et al., 2020; Junttila et al., 2024; Schwarz et al., 2024).

A significant milestone in the adoption of close-range sensing in forest resource mapping is the development of unoccupied aerial vehicles (UAVs) and the sensors they can carry, which has increased the amount of field data that can be collected (Liang et al., 2022). For instance, Kattenborn et al. (2019a) proposed the use of UAVs as an efficient alternative for traditional field sampling in some cases. If the goal is to estimate the spatial coverage of a single species, utilizing plot-based or point-based field sampling data has several challenges, such as spatial inaccuracies and limited spatial coverage. Moreover, acquiring field data is labor intensive and thus costly. UAVs, on the other hand, can provide continuous, georeferenced data (Kattenborn et al., 2019b) in larger quantities than field sampling. Because these data have very high spatial resolution, it is possible for experts to visually identify the target of interest, such as dead canopies or fallen trunks. The data collected with UAVs can then be used as reference data for coarser imagery, such as satellite imagery (Schiefer et al., 2023). Of course, this type of ground reference data has its limitations, as it is only possible to identify objects that are visible from above, and if the target is to measure, e.g., growing stock volume or basal area, additional field work is required.

Depending on the type of deadwood and the remote sensing material used, there are several aspects that affect the accuracy of the deadwood mapping. Using LiDAR point clouds, Heinaro et al. (2021) showed that the amount of undergrowth has a significant effect on the detection of fallen deadwood. Also concerning LiDAR-based deadwood mapping, in Heinaro et al. (2023b), a very high point density resulted in a high number of false positive detections when using line-based detection of fallen deadwood objects. Concerning passive sensors, such as RGB cameras, e.g., the image's spatial resolution, flying altitude and light conditions affect how the forest floor can be observed. Higher altitude results into larger area coverage, but coarser resolution, limiting the size of the targets that can be observed. Also, the amount of overlap between individual images has an effect on how well the forest floor is visible. UAV images are typically captured from low altitudes and high overlap between images, resulting in high spatial resolution, thus enabling detailed observation of forest floor. Nevertheless, the canopy cover percentage still has an impact on what can be detected. Intuitively, the thicker and longer stems are more likely distinguished from the ground as they are more likely to stand out underneath the tree canopies.

Detection of standing deadwood differs significantly from that of fallen deadwood. The standing deadwood with intact crowns are rather trivial to separate from living trees on grounds of object greenness (e.g., Guo et al., 2007; Pasher and King, 2009; Sylvain et al., 2019). On the other hand, standing deadwood with broken or completely missing crowns may be challenging to detect amid dense canopy, especially (Heinaro et al., 2023a). It can also be hard to discern the living trees from the standing dead trees even by visual inspection from the remote sensing data, as tree tops may die due to fungal activity or mechanical damage well before the tree actually dies. This is the case, e.g., in old forests or in forests with a high risk of snow damage.

During the last decade, deep learning and especially convolutional neural networks (CNN) have been increasingly utilized in various remote and close-range sensing studies, ranging from image classification and regression to object detection and different segmentation tasks. The most commonly used approach has been semantic segmentation, in which each pixel in the image is classified into a certain class. These solutions are typically based on U-Net (Ronneberger et al., 2015) and its further iterations. For instance, Schiefer et al. (2020) used this kind of approach for mapping several tree species from high-resolution RGB UAV images, and Jiang et al. (2019) performed deadwood segmentation from false color images, both acquiring excellent results. Semantic segmentation has its downsides, as the produced results do not separate instances without further processing, thus making it difficult to derive other forest characteristics than, e.g., canopy area. Polewski et al. (2021) presented a workflow for separating the individual deadwood instances from semantic segmentation results, acquiring a precision of 0.93, recall of 0.82 and intersection-over-union scores between 0.55 and 0.59.

A well-known bottleneck for utilizing deep learning methods in various forest applications is that these methods require vast amounts of annotated data points for training and validating the models (e.g., Yuan et al., 2020; Kattenborn et al., 2021). This hinders the applications related to scarce forest objects and phenomena, as collecting such datasets with traditional field methods has been simply too costly. Capturing sufficient amount of data requires more and larger field plots than the common and more evenly distributed forest attributes. Nowadays, high-resolution UAV imagery offers a means for collecting very detailed plot-level attributes. Size and number of plots measured with UAVs can be larger, thus covering also more of the scarce and scattered objects, such as deadwood.

Object detection and instance segmentation take the task of detecting objects from images further, as they both detect and classify the objects present in the images. Commonly used methods in the recent years have been Faster R-CNN (Ren et al., 2017) and various iterations of YOLO, You-Only-Look-Once, model family (Redmon et al., 2016; Redmon and Farhadi, 2016, 2018; Bochkovskiy et al., 2020; Jocher et al., 2021, 2023). The main challenge of utilizing bounding box-based object detection in deadwood detection is that fallen trees are long and narrow. These objects might have large bounding boxes, but the object in question only covers a fraction of the bounding box. Moreover, fallen trees can overlap and be densely packed so that bounding boxes of different objects overlap, making post-processing and interpretation of results difficult. Instance segmentation, where the detection model outputs masks for the detections, helps with this problem. Because the training of instance segmentation models requires instance masks, their usage has been limited in vegetation remote sensing (Kattenborn et al., 2021), and has only started to become increasingly used during the last couple of years. Mask R-CNN (He et al., 2020) has been the most popular model type to use in forestry related studies (e.g., Chadwick et al., 2020; de Carvalho et al., 2021; Hao et al., 2021; Chadwick et al., 2022; Hu et al., 2022; Zhang et al., 2022; Chadwick et al., 2024), but recent YOLO versions have also added support for instance segmentation tasks.

In this study, we approached the detection of deadwood through high-resolution drone images that could potentially serve as reference material for large-scale deadwood detection. We first defined the accuracy that can be reached with visual interpretation of high-resolution RGB images. The correctness of manually annotated deadwood objects was evaluated against field-measured reference data. In the second phase, we trained instance segmentation models for automatic interpretation of the images. With this setup we aimed to answer the following questions:

1. How much of the fallen and standing deadwood is it possible to detect from above using optical UAV imagery?

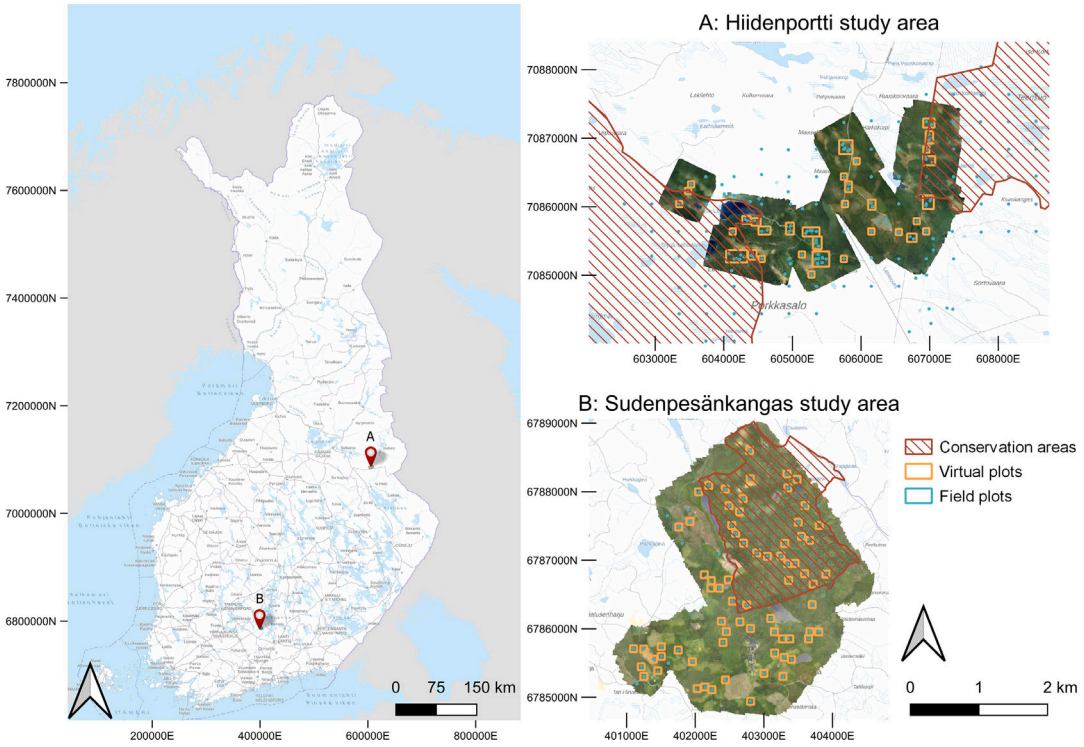

Fig. 1. Locations of the study areas, field plots and scenes.

2. How does canopy cover affect the visibility of fallen deadwood?
3. To what extent can visible deadwood be detected with YOLOv8?
4. How does the composition of training data affect the performance of the instance segmentation model in context of deadwood detection?

2. Materials

2.1. Study areas

We conducted the study in two separate areas. The first area was located in the eastern side of Hiidenportti National Park, Sotkamo, Eastern-Finland, and the field data consisted of both managed and conserved areas (Hiidenportti National Park in the west and Teerisuo - Lososuo area in the east). The most common trees in Hiidenportti area were Scots pine (*Pinus sylvestris* L.) and Norway spruce (*Picea abies* (L.) H. Karst), with different deciduous trees (mainly Silver birch (*Betula pegndula* Roth), Downy birch (*Betula pubescens* Ehrh.), and European aspen (*Populus tremula* L.)). The second study area was located in Sudenpesänkangas, Evo, Southern-Finland. The area covered both managed and conserved forests, and the canopy was mostly dominated by Scots pine and Norway spruce, with a mixture of Silver birch and Downy birch. Other species (e.g., European aspen and larch) were rather scarce in the dominant canopy layer. The geographical location for both study areas, as well as field plots and conservation areas is shown in Fig. 1.

2.2. UAV and LiDAR data

The UAV data from the Hiidenportti study area consisted of nine partially overlapping RGB orthoimages which covered an area of approximately 10 km^2, with a spatial resolution ranging between 3.9 cm and 4.4 cm. These images covered both conserved and managed forests, as well as some logging openings. The UAV images were collected on 16.–17.7.2019 using a DJI Phantom 4 RTK UAV equipped with a 20 megapixel CMOS sensor and a real-time kinematic (RTK) GNSS receiver (DJI, Shenzhen, China). The flight altitude was set to 130 m above ground level and the image acquisition was carried out with 80% front and side overlap to ensure sufficient quality of resulting orthomosaics.

The UAV images from the Sudenpesänkangas study area covered approximately 12 km^2 and were acquired on 11.7.2018, using the eBee Plus RTK fixed-wing platform, equipped with a 20 megapixel global shutter S.O.D.A camera (SenseFly SA, Cheseaux-sur-Lausanne, Switzerland). The UAV imagery consisted of a single RGB orthomosaic with a spatial resolution of 4.9 cm. The flight altitude was set to 150 m above ground level. Image acquisition was performed with a front and side overlap of 85% to ensure high-quality reconstruction. More details about the UAV imagery and field plots at the Sudenpesänkangas study area can be found in Kuzmin et al. (2021).

UAV images were processed in Agisoft Metashape (Agisoft LLC, St. Petersburg, Russia), which uses Structure from Motion (SfM) to generate georeferenced products from overlapping images. The main focus was on creating high-quality RGB orthomosaics, with point clouds also produced during processing. Image alignment was performed at full resolution using the “high quality” setting, with camera calibration based on Brown’s distortion model. Then a dense point cloud was generated using downsampled images (factor 4) and “Mild” depth filtering. RGB orthomosaics were created by orthorectifying the images over a digital elevation model (DEM) derived from the dense point cloud. The final mosaics were geometrically corrected and radiometrically consistent.

In addition to UAV images, we also utilized canopy height model (CHM) derived from high-resolution airborne LiDAR data in Hiidenportti study area. These LiDAR data for Hiidenportti area were collected on 17.5.2019 with mean point density of approximately 15 points/m^2, and more accurate details for them can be found in Heinaro et al. (2021). In this study, we used these data to estimate how much of the field-measured deadwood is even possible to detect from above, and how the canopy cover percentage for the field plots affects it. The percentage was determined as a relative share of a plot area covered with at least 2 m high vegetation.

2.3. Field data

The field data for this study were collected during multiple projects. For Hiidenportti study area, the data were collected as circular field plots with 9 m radius during three separate campaigns. In campaign 1, 45 field plots were measured between July and August 2019. The UAV images were collected as a part of campaign 1, so only the plots from that campaign were guaranteed to be covered. In campaign 2, 103 plots were measured in July-September 2019 (Heinaro et al., 2021), and in campaign 3, 30 plots were measured in November 2020 (Heinaro et al., 2023a). Both living and dead trees were measured from all the plots. For all living trees with diameter at breast height (DBH) of 45 mm or more, DBH, height, species, and location in relation to the plot center (azimuth angle and distance) were recorded. As for the trees with DBH under 45 mm, species level mean values of DBH and height were recorded. The measurement procedures differed between campaigns for fallen deadwood. In all campaigns the diameter cutoff of the thickest part of fallen trunks was set to 100 mm. In campaign 1 only the parts of fallen deadwood that were inside the plots were measured. The stem diameter was determined from the center of the trunk sections within the plots. In campaigns 2 and 3, the measurements were more detailed as all fallen deadwood trunks touching the plot area were fully measured. The locations of both ends of the trunks were also measured using a Trimble R2 RTK-GNSS device (Trimble Inc., Sunnyvale, California, USA), which allowed determining the deadwood sections within the plots in the post-processing phase, as well as estimating how much of the fallen deadwood could be seen from above.

In order to have similar diameter information in each of the three campaigns in Hiidenportti, the diameter at the central part of the fallen trees was estimated by first estimating the diameter of the base of the trunk with the formula from Laasasenaho (1975), and then considering the trunks as either right or truncated circular cones for further computations. Out of the 178 circular field plots with 9 m radius present in the Hiidenportti area, our UAV images covered 75 in such way that the image quality was sufficient for our study. Out of these 75, we omitted four plots as they were located in clear-cut areas, bringing the total number of field plots to 71: 41 from campaign 1, 19 plots were from campaign 2 and 11 from campaign 3. Ten of these plots did not contain any field-measured deadwood.

The field data for Sudenpesänkangas were collected during the summer of 2018, as a part of a larger field campaign (for details, see Viinikka et al. (2020) and Mäyrä et al. (2021). In the campaign, the field plots were distributed using stratified sampling, according to the main tree species, DBH, and basal area from compartment-level forest inventory data from 2015. Each standing tree, with DBH of at least 45 mm was measured. Deadwood was not measured in the field in this campaign. Our UAV images covered 71 field plots with suitable image quality for our use cases.

2.4. Annotated deadwood data

As using only field-measured data would not have provided enough training data for our methods, we manually annotated the data based on visual interpretation. For both of our study areas, we extracted rectangular areas from the UAV mosaics (hereafter referred as *scenes*) around the field plots, so that the scenes were placed around every usable field plot. Because the dimensions of the UAV mosaics were different between the study areas, these scenes were constructed slightly differently. For the Hiidenportti dataset, we constructed 33 rectangular scenes by first buffering each plot center with a 45 m square buffer, resulting in 90 × 90 m squares corresponding to each plot, and then creating rectangular areas from the overlapping squares (Fig. 2). In cases where multiple UAV mosaics covered one scene, only one mosaic was used as the reference image for the corresponding location. In Sudenpesänkangas, the field plots were located more sparsely, and we could construct the scenes as 100 × 100 m non-overlapping squares. We constructed all scenes in such a way that each contained only one circular field plot.

We manually annotated all visible deadwood from the extracted scenes to use them as our training and validation data. The standing deadwood instances were annotated so that the full canopies were inside the polygons, but for fallen deadwood we annotated only the trunks and left the branches unannotated. Both types of deadwood were annotated as separate classes. All visible deadwood was annotated regardless of its length, as it was possible that, in reality, they belonged to a larger trunk but were partially obscured by the canopy. Examples of annotated deadwood from both study areas are shown in Fig. 3.

In addition to the total number of deadwood instances, the annotated deadwood data indicate the total area covered by each deadwood type. Based on the annotated polygons, we also estimated the trunk length of the fallen deadwood and the maximum canopy diameter of the standing deadwood. Both were defined as the longest side of the minimum rotated rectangle for the corresponding polygon. For diameter estimation of the fallen deadwood, we constructed three lines perpendicular to the minimum rotated rectangle of the polygon that intersect it at 10%, 50% and 90% lengths (Fig. 4). Based on these lines, we used their mean length to estimate the polygon diameter. As the diameter estimates were rather coarse, we did not use them to characterize individual fallen trees, but rather to get an overall idea of what diameter classes of fallen deadwood were present in the area.

In total, we annotated 13,813 deadwood instances, of which 2502 were standing deadwood canopies and 11,311 were fallen deadwood trunks. Hiidenportti dataset contained 1083 standing and 7396 fallen annotations, whereas Sudenpesänkangas contained 1419 standing and 3915 fallen annotations. The annotated fallen deadwood instances were around a meter longer, and the standing deadwood canopies covered over twice as much area in Sudenpesänkangas than in Hiidenportti. Most of the annotated data were located in managed forests. It is worth mentioning that a large number of annotated fallen deadwood instances were shorter than 1.3 m (the minimum length for the tree to be measured in the National Forest Inventory) in both study areas, but due to the possibility of them being larger trunks that were partially obscured by the canopy, they were included in the dataset. Summary of the annotated data is shown in Table 1.

2.5. Instance segmentation datasets

We constructed three separate datasets from our annotated deadwood data: one consisting only of Hiidenportti data (HP), one consisting only of Sudenpesänkangas data (SPK) and one consisting of both study areas (combined). We split each dataset into three separate subsets spatially, so each scene was only used in either the train, validation, or test set. The spatial locations of the train, validation, and test images were set so that they were consistent in each dataset (e.g., same images from Hiidenportti were used for testing HP dataset and combined dataset), shown in Fig. 5. This enabled us to evaluate how the models were transferable between locations, as well as to assess whether also using data from other areas improved the results compared to using data only from the same area.

As using the full-sized scenes for training the models would be unfeasible due to their large sizes, the images were split into 640 ×640 pixel image chips without overlap, and the georeferenced polygon annotations were converted to YOLO annotation format. After this process, the HP dataset contained 632 image chips for training, 142 for validating, and 211 for testing. The SPK dataset contained 688, 224, and 224 chips for training, validating, and testing, respectively.

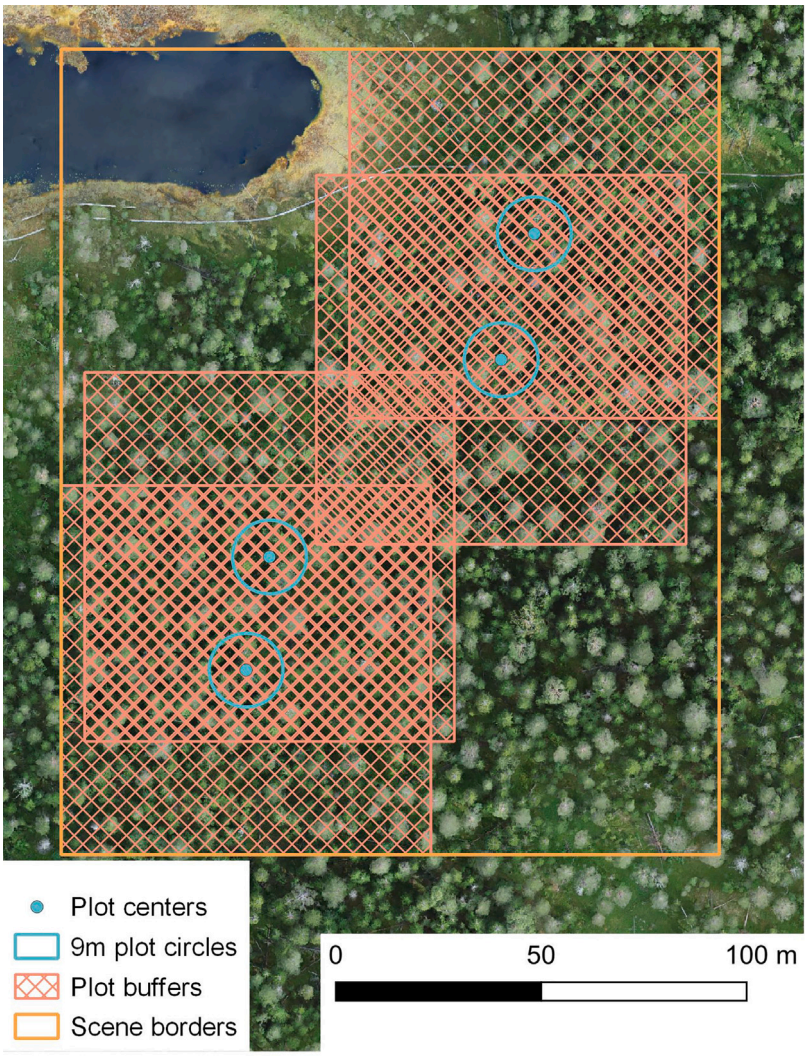

Fig. 2. Example on how scenes for Hiidenportti were constructed. There is a 45 m distance from each plot center to the edge of the rectangular scene.

Table 1
Summary of annotated deadwood characteristics.

	Hiidenportti			Sudenpesänkangas		
	Managed	Conserved	Total	Managed	Conserved	Total
Total number of standing deadwood	683	400	1083	386	1033	1419
Total number of fallen deadwood	5909	1487	7396	2373	1542	3915
Total standing deadwood area (m^2)	2104.13	1461.61	3565.37	1212.99	6003.06	7216.05
Total fallen deadwood area (m^2)	2531.89	936.92	3459.81	1547.97	1606.20	3154.17
Mean fallen deadwood length (m)	2.28	2.88	2.40	3.13	3.89	3.43
Total fallen deadwood length (m)	13 501.6	4283.6	17 785.2	7432.7	5994.3	13 427.0
Mean fallen deadwood diameter (mm)	180.40	208.54	186.06	200.59	254.21	221.71

3. Methods

3.1. Instance segmentation methods

The main advantage of using instance segmentation (detecting and segmenting the accurate masks for objects) instead of only bounding-box-based object detection is the additional information, e.g., instance diameter estimates, that can be derived from the masks compared to the bounding boxes, especially for fallen deadwood instances. As these are typically long and narrow, fallen trunks that are diagonal in the image have large bounding boxes even though the object in question covers only a small fraction of it. Also, as overlapping detections are typically eliminated during post-processing, utilizing methods based only on bounding boxes might remove otherwise correct detections.

We used Ultralytics YOLOv8 (Jocher et al., 2023) as the instance segmentation framework for this task, as it was considered to be one of the best performing instance segmentation models at the time this study was conducted. There are five different architectures of YOLOv8 segmentation models available with different number of parameters. A higher number of parameters typically corresponds to better results, but slower training and inference. We trained a total of fifteen different variations of the models, so that each architecture was fitted with each of our datasets. The models were trained for a maximum of 300 epochs using early stopping tolerance of 50 epochs, meaning that if the validation results did not improve during that time the training was stopped. During training, the input images were augmented using random flips and scaling, random HSV-adjustments, random crops and mosaic augmentations. Batch sizes for the models were automatically

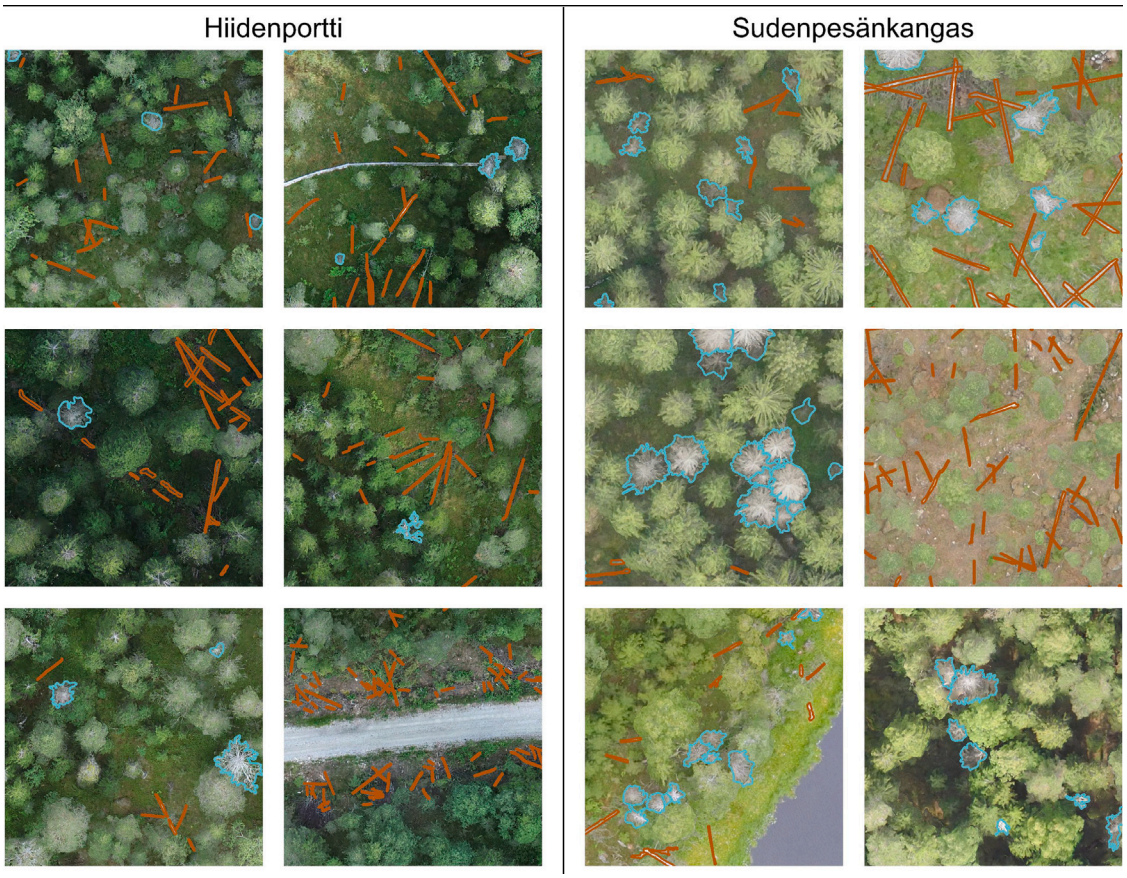

Fig. 3. Examples on the annotated deadwood instances from both study areas.

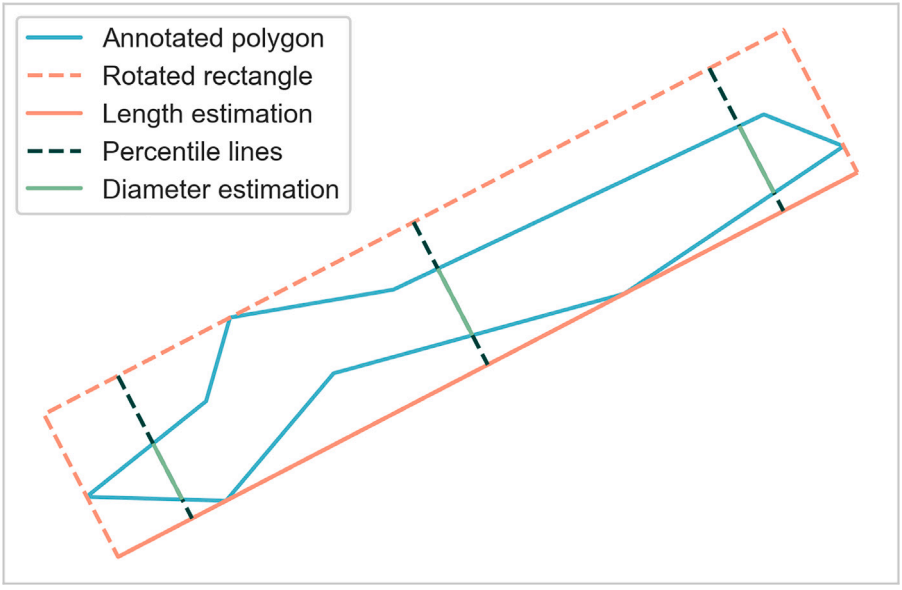

Fig. 4. Visualization of the length and diameter estimation for the fallen deadwood. Length of the light green polygon is estimated with the length of unified light red line, and the diameter is estimated as the mean length of the three light green lines. (For interpretation of the references to color in this figure legend, the reader is referred to the web version of this article.)

chosen to be so large that they consumed a maximum of 60% of the available GPU memory. Weights & Biases (Biewald, 2020) was used to track the model metrics. We used a single NVIDIA V100 GPU with 32 GB of memory, hosted on computing nodes of Puhti supercomputer hosted by CSC – IT Center for Science, Finland. All used codes and examples of the analyses done are available in https://github.com/mayrajeo/yolov8-deadwood, and all trained models are available in https://huggingface.co/mayrajeo/yolov8-deadwood.

For inference, we used SAHI (Akyon et al., 2022) library to generate the predictions for the larger scenes. The scenes were sliced into 640 × 640 pixel image chips with an overlap ratio of 0.2, and processed the resulting tiles with slightly modified version of greedy

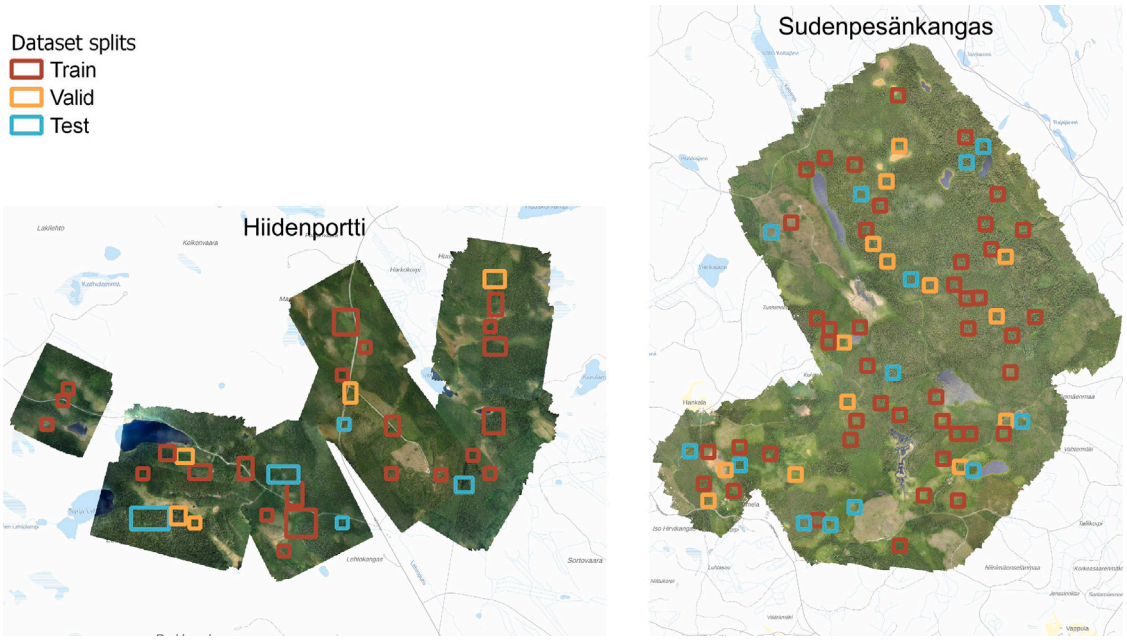

Fig. 5. Spatial splits for the dataset.

non-maximum merging from the SAHI library. We modified the algorithm to work with georeferenced polygon data, and repeated the process until no more polygons were merged, using Intersection-over-Smaller area (IoS) threshold of 0.2. IoS is the ratio of the intersection area and the area of the smaller object of two targets.

3.2. Evaluation

3.2.1. Estimating the amount of exposed fallen deadwood

As campaigns 2 and 3 from Hiidenportti contained RTK-measured fallen deadwood data, we utilized them to evaluate how much of the fallen deadwood was even possible to see from above. We used the CHM from Hiidenportti and all field data from these campaigns that overlapped with the CHM, a total of 129 field plots, to quantify the amount of exposed fallen deadwood, regardless of whether they were covered by UAV images. We defined the parts of fallen deadwood to be exposed if they were not covered by CHM with height more than 2 m. This process is visualized in Fig. 6. We quantified the amount exposed by comparing the total length of exposed fallen deadwood to the within-plot total length of all field-measured fallen deadwood.

3.2.2. Comparing annotations and predictions with field data

In order to estimate how well the predictions compare to the field data, we evaluated the annotations and predicted deadwood instances by comparing them to the plot level data in Hiidenportti. We determined the accuracy of the annotated data by comparing them to the total number of both deadwood types (i.e., standing and fallen), and to the within-plot total length and mean diameter of fallen deadwood. Also, we used similar comparisons to compare the predictions with the field data and to evaluate their quality. All comparisons were made using the data aggregated at the plot level. For the within-plot lengths, we used only the data from campaigns 2 and 3. These data contained 21 field plots with field-measured fallen deadwood, and 7 of these were contained in the test partition of our dataset.

3.2.3. Instance segmentation performance

While evaluating the performance of an object detection or an instance segmentation model, the evaluation metrics must be selected so that both the localization accuracy and the classification accuracy are taken into account. The key metric to define whether a prediction

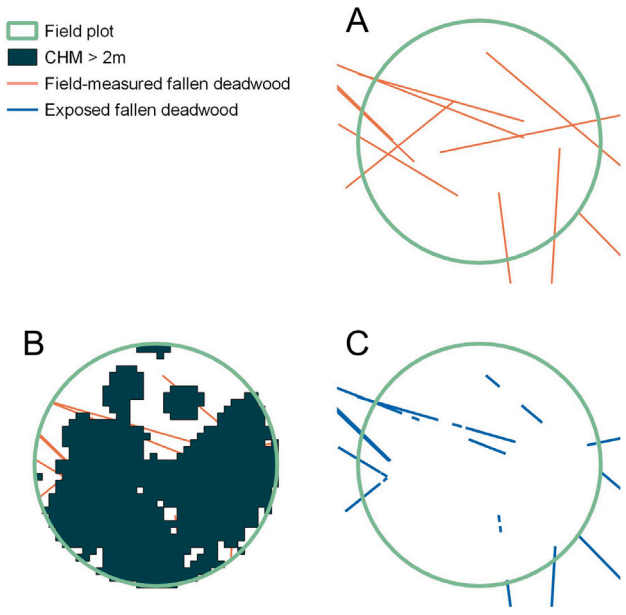

Fig. 6. Visualization on how the field-measured fallen deadwood were defined to be exposed. A: All field-measured fallen deadwood for a single field plot. B: Field-measured deadwood within the plot circle, overlaid with CHM with value of at least 2 m. C: Parts of fallen deadwood defined as exposed.

is correct or not is **Intersection-over-Union (IoU)**, which is the ratio of the area of intersection and area of union of two masks. IoU of 1.0 indicates perfect overlap and 0.0 no overlap at all. This metric is also typically used to evaluate semantic segmentation models.

Each predicted mask is compared with each of the available target masks for a given input. The result is defined as a **true positive (TP)** when a prediction mask and a ground truth mask have IoU exceeding some predefined threshold, a **false positive** when a predicted mask has no associated ground truth mask and a **false negative** when a ground truth mask has no associated predicted mask. As each image has infinite number of different masks that have no corresponding ground truth, there are also infinite number of **true negatives (TN)**

and thus TN is not relevant type of result for these tasks. In the case of multiple detections having larger IoU than the threshold with a ground truth mask, the prediction with the highest prediction confidence is considered to be TP and others FN.

With TP, FP, and FN, it is possible to derive the two primary metrics: **Precision** and **Recall**. Precision is the ratio of TP and all detections and recall is the ratio of TP and all ground truths. By varying the confidence threshold for a prediction being correct, it is possible to plot precision as a function of recall (**Precision-Recall curve**). The area under this curve is known as **Average Precision (AP)**, and it is often computed with the 11-point interpolation method, defined as

$$AP = \frac{1}{11} \sum_{recall \in R} p(r), \; R = [0.0, 0.1, \ldots, 0.9, 1.0]$$

where

$$p(r) = max(Precision(r')), r' \leq r$$

In order to get more accurate indication of the model performance, AP is computed with multiple IoU thresholds. For instance, in the COCO object detection challenge (Lin et al., 2014), the evaluation metrics include AP with IoU thresholds 0.5 (**AP50**), 0.75 (**AP75**), and AP averaged over ten IoU thresholds [0.5, 0.55, … , 0.9, 0.95] (**AP [.50:.05:.95]** , **mAP** hereafter), which is the main challenge metric. These metrics can also be computed separately for different object sizes, typically small (bounding box smaller than 32^2 pixels), medium (bounding box between 32^2 and 96^2 pixels) and large (bounding box larger than 96^2 pixels). In this study, we used precision, recall, AP50 and mAP to evaluate the object detection performance of the models. The IoU threshold used for deriving precision and recall was 0.5. We used both AP50 and mAP as the instance segmentation metrics as they are the most commonly used among object detection and instance segmentation metrics. Using both of these metrics also gives us more comprehensive information about the model performance, as AP50 shows the general, fairly lenient localization performance, and mAP shows how well the masks are delineated compared to the ground truth. Also, as almost all of our targets are considered "small" by COCO definitions, we did not evaluate the results using different scales.

In addition to the aforementioned metrics, we also compared the characteristics of the detected deadwood with the annotations for the test set from both study areas. These characteristics include the total numbers of both types of deadwood, the total area covered by them, the mean diameter and length, as well as the total length of the fallen deadwood.

4. Results

4.1. Comparison between field data and human annotated data

In this section, we first quantify how much of the fallen deadwood was possible to see from above based on the individually measured fallen deadwood and the CHM. We then compare the field data measurements and manually annotated deadwood data within the 9 m circular plots. All fallen deadwood lengths and diameters for the annotated data presented in this section are derived from the parts within the circular plots. These results reflect how much of the field-measured data could be seen from UAV imagery. We used only Hiidenportti data to do these comparisons, as we did not have individually measured deadwood field data from Sudenpesänkangas.

The effect of canopy cover on fallen deadwood visibility in Hiidenportti was such as expected. Higher canopy cover percentage corresponded to less deadwood being exposed. On average, around 46% of the field-measured fallen deadwood was exposed, and the average canopy cover percentage for the field plots was around 58%. The canopy also fragmented the deadwood into multiple parts, so that the number of fallen deadwood instances typically increased. These plot-wise comparisons are shown in Fig. 7. The average length of exposed deadwood segments was around 1.45 m, whereas the average length of field-measured trunks was more than 6.6 m.

Compared to field-measured deadwood within plots, we annotated less standing deadwood than present in the field for both forest types and less fallen deadwood than were measured in the field for conserved forests. However, in managed forests the number of annotated deadwood instances was around 14% higher than the number of deadwood measured in the field. As the resolution of our data made it impossible to accurately tell whether a fallen trunk had a diameter less than 100 mm, some of the annotations can be such that they were determined to be below the threshold diameter in the field.

As expected, the field-measured fallen deadwood tunks were longer than annotated deadwood instances. Most of the annotated fallen deadwood were shorter than 2 m, while the field-measured fallen deadwood trunks were typically longer than 5 m. However, this is most likely due to the fragmentation of the fallen deadwood due to blockage of dense canopies on the image, which resulted in some of the longer trees to be annotated as multiple shorter ones. When comparing the difference of total lengths of field-measured trees and annotated trees, a higher canopy cover percentage (i.e., denser canopy) typically meant a larger difference. When comparing the diameter distributions for fallen deadwood, the diameter classes 125–150 mm, 150–175 mm and 175–200 mm were over-represented in the annotated data. As these diameter classes were also the most common among the field data, this might be due to single trunks being annotated as multiple polygons. A summary of these comparisons is shown in Table 2.

When comparing only the exposed parts of the fallen deadwood with the annotations (Fig. 8) for the field plots from campaigns 2 and 3, we noticed that we were able to annotate less fallen deadwood than what should be exposed, both with respect to individual instances and the total length. However, the differences between the total lengths of the fallen deadwood were not as extreme as with the total numbers of instances.

4.2. Deadwood segmentation performance

In this section, we present the deadwood segmentation results and compare how the annotated dataset used for training affected the results for each location. We also evaluated which of the YOLOv8 segmentation model architectures had the best deadwood segmentation performance according to the metrics. Based on these results, we selected the best performing model and used it to generate results for further analyses.

For the Hiidenportti dataset, models trained with only Sudenpesänkangas data performed worse than models trained with either Hiidenportti data or data from both sites (Table 3). The differences were more noticeable for standing deadwood, as there was a difference between 0.15 and 0.2 in AP50 for each model architecture. Also, models trained with the combined dataset outperformed the models trained with only Hiidenportti data, especially on standing deadwood.

The results for Sudenpesänkangas dataset (Table 4) revealed similar results as for Hiidenportti, so that the models trained with only Hiidenportti data were clearly the worst performers. The differences were even greater compared to the results from Hiidenportti dataset, with a difference of around 0.3 for standing deadwood AP50 and 0.2 for fallen deadwood AP50. Models trained with the combined dataset were also the best performing here, with slightly better results for both classes.

Overall, the different model architectures performed mostly according to their number of parameters, so that the smallest model, yolov8n, had the lowest AP50 and mAP50 scores and the largest models, yolov8l and yolov8x, had the highest. The training times varied between 10 min (yolov8n with Hiidenportti dataset) to around three hours (yolov8x with combined dataset).

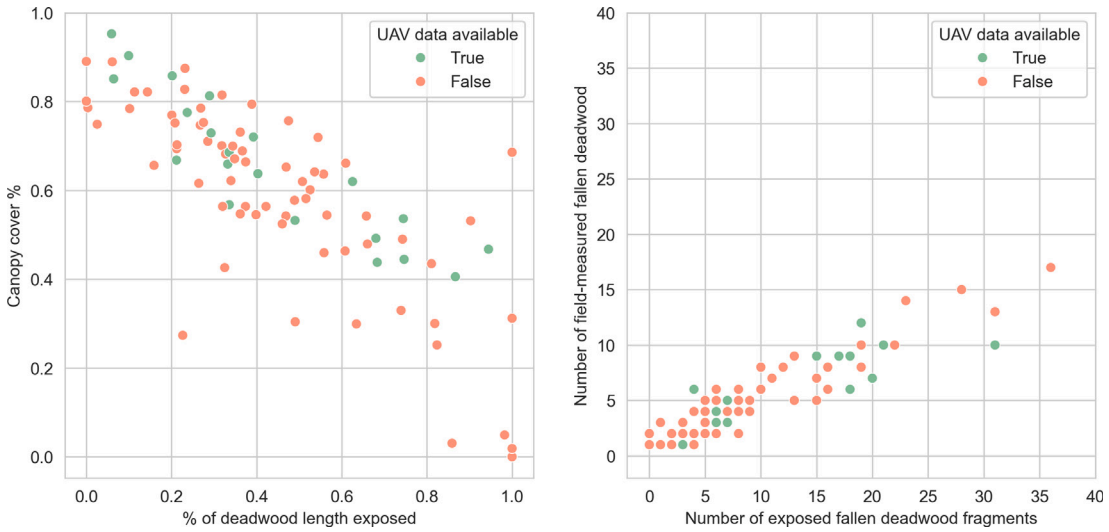

Fig. 7. Left: Comparison of canopy cover percentage and the percentage of field-measured exposed fallen deadwood length. Right: Comparison of the number of field-measured fallen deadwood and the number of exposed deadwood fragments.

Table 2
Comparison between annotations and field data for Hiidenportti dataset.

	Managed		Conserved		Total	
	Field	Annotations	Field	Annotations	Field	Annotations
Number of standing deadwood	75	49	24	10	99	59
Number of fallen deadwood	217	248	96	48	313	296
Mean fallen diameter (mm)	133.8	175.0	185.5	208.4	149.7	181.2
Min fallen diameter (mm)	15.6	16.6	39.2	27.32	15.6	16.6
Max fallen diameter (mm)	450	381.3	580.6	625.9	580	625.9
Mean fallen length (m)	6.8	1.8	7.6	2.1	7.0	1.9
Min fallen length (m)	0.5	0.1	0.2	0.2	0.2	0.1
Max fallen length (m)	16.7	6.5	18.0	5.9	18.0	6.5
Total fallen length (m)	1468.8	429.3	728.5	125.0	2197.3	554.3

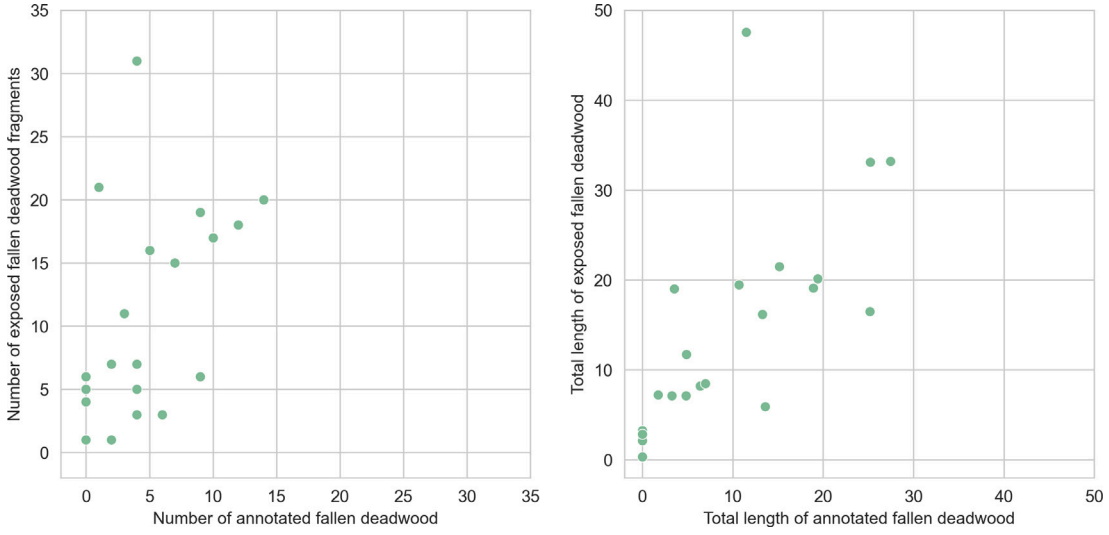

Fig. 8. Left: Comparison between the number of exposed fallen deadwood fragments and the number of annotations. Right: Comparison between the total length of exposed fallen deadwood and the total length of annotated fallen deadwood.

4.3. Comparisons between annotations and predictions

In this section, we compared the annotations and predictions in the test scenes from both study areas. The predictions were filtered so that all polygons that were shorter than 0.3 m or had a diameter less than 50 mm were discarded, as these detections were most likely artefacts from the slicing process. For the Hiidenportti test set, the predicted fallen deadwood instances were on average slightly thicker and shorter compared to annotations, and the predicted standing deadwood canopies were a little larger than annotated. Compared to human annotators, the predictions detected around the same total number of both types of deadwood, though there were several false positives and false negatives. Comparisons between annotations and predictions are shown in Table 5.

Table 3
Results for Hiidenportti dataset. HP: Data from Hiidenportti. SPK: Data from Sudenpesänkangas. Both: Data from both sites.

		Precision			Recall			AP50			mAP		
		Total	Fallen	Standing	Total	Fallen	Standing	Total	Fallen	Standing	Total	Fallen	Standing
Model	Trainset												
yolov8n	HP	0.591	0.624	0.557	0.575	0.571	0.579	0.600	0.602	0.598	0.294	0.273	0.315
	SPK	0.512	0.560	0.463	0.469	0.485	0.454	0.464	0.495	0.433	0.198	0.194	0.202
	Both	0.720	0.741	0.699	0.571	0.534	0.607	0.647	0.612	0.683	0.317	0.263	0.371
yolov8s	HP	0.688	0.679	0.697	0.581	0.563	0.599	0.643	0.613	0.672	0.325	0.280	0.370
	SPK	0.548	0.669	0.428	0.478	0.463	0.492	0.484	0.528	0.439	0.212	0.213	0.211
	Both	0.650	0.623	0.678	0.614	0.644	0.584	0.656	0.638	0.675	0.324	0.284	0.364
yolov8m	HP	0.683	0.678	0.688	0.572	0.570	0.574	0.638	0.607	0.669	0.306	0.256	0.356
	SPK	0.609	0.702	0.516	0.563	0.539	0.587	0.551	0.591	0.512	0.256	0.254	0.258
	Both	0.676	0.643	0.710	0.619	0.637	0.602	0.671	0.638	0.703	0.338	0.286	0.390
yolov8l	HP	0.673	0.642	0.704	0.572	0.611	0.533	0.624	0.599	0.648	0.302	0.256	0.348
	SPK	0.609	0.700	0.518	0.530	0.524	0.536	0.544	0.585	0.504	0.254	0.254	0.253
	Both	0.701	0.658	0.744	0.622	0.627	0.616	0.676	0.648	0.705	0.339	0.291	0.386
yolov8x	HP	0.656	0.607	0.705	0.600	0.614	0.587	0.635	0.630	0.640	0.317	0.285	0.350
	SPK	0.550	0.706	0.395	0.493	0.460	0.526	0.469	0.548	0.390	0.211	0.234	0.188
	Both	0.709	0.684	0.734	0.620	0.603	0.638	0.682	0.654	0.709	0.353	0.306	0.400

Table 4
Results for Sudenpesänkangas dataset. HP: Data from Hiidenportti. SPK: Data from Sudenpesänkangas. Both: Data from both sites.

		Precision			Recall			AP50			mAP		
		Total	Fallen	Standing	Total	Fallen	Standing	Total	Fallen	Standing	Total	Fallen	Standing
Model	Trainset												
yolov8n	HP	0.683	0.492	0.873	0.233	0.249	0.218	0.308	0.288	0.329	0.138	0.106	0.170
	SPK	0.721	0.615	0.826	0.519	0.491	0.547	0.591	0.508	0.673	0.292	0.197	0.388
	Both	0.730	0.682	0.778	0.527	0.444	0.611	0.604	0.504	0.705	0.305	0.198	0.413
yolov8s	HP	0.586	0.446	0.726	0.342	0.347	0.336	0.414	0.331	0.497	0.187	0.121	0.253
	SPK	0.670	0.634	0.706	0.609	0.517	0.702	0.638	0.537	0.739	0.310	0.206	0.413
	Both	0.672	0.617	0.727	0.577	0.508	0.646	0.617	0.526	0.709	0.309	0.209	0.410
yolov8m	HP	0.613	0.440	0.786	0.339	0.330	0.349	0.407	0.331	0.482	0.185	0.122	0.248
	SPK	0.720	0.604	0.835	0.556	0.529	0.583	0.635	0.525	0.744	0.317	0.215	0.420
	Both	0.716	0.639	0.792	0.581	0.515	0.647	0.646	0.535	0.757	0.336	0.225	0.447
yolov8l	HP	0.573	0.414	0.732	0.340	0.366	0.313	0.397	0.328	0.465	0.162	0.113	0.212
	SPK	0.709	0.641	0.777	0.584	0.501	0.667	0.639	0.530	0.748	0.332	0.223	0.442
	Both	0.750	0.678	0.822	0.572	0.520	0.623	0.656	0.559	0.753	0.341	0.240	0.441
yolov8x	HP	0.675	0.543	0.807	0.322	0.362	0.282	0.421	0.385	0.457	0.185	0.141	0.229
	SPK	0.680	0.669	0.691	0.597	0.483	0.711	0.624	0.516	0.731	0.308	0.202	0.415
	Both	0.711	0.663	0.760	0.611	0.554	0.667	0.651	0.556	0.746	0.333	0.234	0.432

Table 5
Comparison between annotated data and predictions for Hiidenportti test dataset.

	Managed		Conserved		Total	
	Annotated	Predicted	Annotated	Predicted	Annotated	Predicted
Number of standing deadwood	181	206	159	172	340	378
Number of fallen deadwood	916	889	485	439	1401	1328
Mean fallen diameter (mm)	194.4	208.1	220.9	232.21	203.6	216.1
Mean fallen length (m)	2.6	2.6	3.2	2.7	2.8	2.7
Total fallen length (m)	2401.0	2364.7	1556.2	1210.1	3957.2	3574.8
Total fallen area (m^2)	479.58	510.25	360.00	296.57	839.58	806.82
Mean standing canopy area (m^2)	3.06	3.16	4.06	4.16	3.53	3.62
Total standing canopy area (m^2)	555.1	651.6	645.7	716.8	1200.8	1368.5

In Sudenpesänkangas (Table 6), the number of fallen deadwood was underestimated in conserved forests and the number of standing deadwood was slightly overestimated. The predicted fallen deadwood were on average a bit shorter than the annotations, and the estimated mean diameter was around 30 mm larger. For standing deadwood, the average canopy area of the predictions was larger compared to the annotations, as the total area covered by the predicted standing deadwood canopies was almost 200 m^2 more than the area covered by the annotations, although there were only 20 more predicted instances than the annotations.

4.4. Comparison between field data and predicted deadwood instances

In order to estimate the operational accuracy of the method, we compared the predicted deadwood instances with the field-measured reference data. In Hiidenportti, the test dataset contained 15 circular

Table 6
Comparison between annotated data and predictions for Sudenpesänkangas dataset.

	Managed		Conserved		Total	
	Annotated	Predicted	Annotated	Predicted	Annotated	Predicted
Number of standing deadwood	72	82	140	150	212	232
Number of fallen deadwood	691	612	251	210	942	822
Mean fallen diameter (mm)	192.3	223.5	233.1	272.9	203.2	236.1
Mean fallen length (m)	2.9	2.7	3.4	3.3	3.0	2.8
Total fallen length (m)	2010.0	1646.6	844.1	688.0	2854.1	2334.6
Total fallen area (m^2)	391.93	387.37	200.93	194.54	592.86	581.91
Mean standing canopy area (m^2)	3.98	4.27	4.30	4.64	4.19	4.51
Total standing canopy area (m^2)	286.3	350.4	602.5	696.0	888.8	1046.5

Table 7
Comparison between the field-measured, annotated and detected fallen deadwood for the field plots with individually measured fallen deadwood in the test set.

Plot ID	Canopy cover %	Fallen deadwood count			Fallen deadwood length (m)		
		Exposed	Annotated	Detected	Exposed	Annotated	Detected
106	0.532	31	4	7	47.5	11.5	13.1
117	0.775	16	5	4	11.7	4.9	5.0
131	0.720	17	10	9	20.1	19.4	18.5
1021	0.729	7	2	1	7.2	1.7	1.7
1025	0.405	1	2	2	7.1	4.8	4.7
1036	0.638	19	9	6	19.5	10.7	10.1
1053	0.445	3	6	3	5.9	13.6	9.9

field plots, of which 6 were in conserved forests and 9 in managed forests. There were only two plots in which the model overestimated the number of standing deadwood compared to field measurements and same was true also for fallen deadwood. Seven of the field plots present in the test dataset had individually measured fallen deadwood data. The predictions aligned fairly well with the annotations within the field plots, but underestimated both the total number and the total length compared to the field data (Table 7).

Fig. 9 shows the visual comparisons of field measurements, annotations, and predictions for three of the field plots. In each of these plots, there were several fallen deadwood trunks that were not visible from above due to canopy cover. In plot 1036 the total within-plot lengths of both annotated and detected fallen deadwood trunks were around half of the field measurements, and in plot 106 the total within-plot length of the annotated or predicted fallen deadwood were less than a quarter of the total exposed length (Table 7). Also, while the total length of the deadwood from different sources was almost identical in plot 131, visual inspection revealed that the locations of the annotated or detected fallen deadwood instances were considerably different compared to field data. Not all standing deadwood were visible either, as in plot 1036 there was a single standing dead tree with its top missing which was undetected by both experts and model, and in plot 106 there were two standing dead trees which were below higher living canopy. Most of the exposed parts of fallen deadwood trunks were detected, but depending on the field plot, matching them with field measurements was not straightforward, as the measurements and UAV mosaics did not align perfectly.

5. Discussion

In this study, our aim was to present a method to utilize UAV images for improved deadwood mapping and assess how trustworthy the results are compared to field data. We also assessed the roles of the RGB data, canopy cover, the YOLOv8 object detection method used, and the composition of training data in the detection process.

5.1. Viability of RGB UAV images in deadwood detection

Our results from the visual annotation show that about 60% of the standing deadwood could be detected from the UAV images, as for fallen deadwood the annotation rate was about 25% (of the total field measured deadwood length) (Table 1). However, in nearly all of the field plots, the number of exposed fallen deadwood fragments greatly exceeded the number of field-measured trees (Fig. 7). Also, the annotated mean diameter for the fallen deadwood was over 20% bigger than in the field data. This indicates that the largest deadwood trunks were more likely to be annotated and that the share of annotations from the actual deadwood volume was significantly higher than the detection of 25% of total length suggests. Of course, it is impossible to accurately estimate the diameter of the objects from the UAV images, as the spatial resolution limits the accuracy of the delineations for both expert annotators and automatic methods.

According to our inspection, the visible share of fallen deadwood decreases almost linearly as the canopy cover percentage increases (Fig. 7). However, the canopy also affected the detection in other ways. The standing canopy limits the visibility from above and splits long stems into several shorter ones. In our study, this resulted in less annotated deadwood length overall, but higher number of exposed deadwood fragments (Fig. 7). Typically, the amount of exposed downed deadwood fragments was about double of the actual field-measured fallen deadwood (Fig. 7). Based on visual interpretation, the overestimates were largely caused by the living canopies blocking the view to the fallen deadwood and thus splitting them into multiple parts (Fig. 9). This observation is also supported by the short length of average annotated deadwood instances, since the mean length of the annotated fallen trees was nearly 80% shorter than the mean length of the field-measured fallen deadwood.

The reasons for some of the downed deadwood trunks remaining undetected are diverse. In addition to the living canopy discussed above, also the vegetation at the ground level likely affects the detection. In our field data, many of the oldest trunks were at least partly covered with mosses, which made their spectral characteristics very similar to those of the forest floor. This may be one of the reasons for smallest diameter fractions of fallen deadwood remaining undetected both in the annotation and the prediction phases. The small-diameter trunks are more rapidly overgrown by ground vegetation, but also have smaller surface area that could be discerned from optical images. Thus, along with canopy conditions and ground vegetation, also the image resolution likely plays an important role when considering the detection rate of the smallest diameter classes.

As for standing deadwood, the biggest challenge was that branchless snags are almost impossible to detect from above. Even in high-resolution UAV imagery, they often cover only a couple of pixels, and

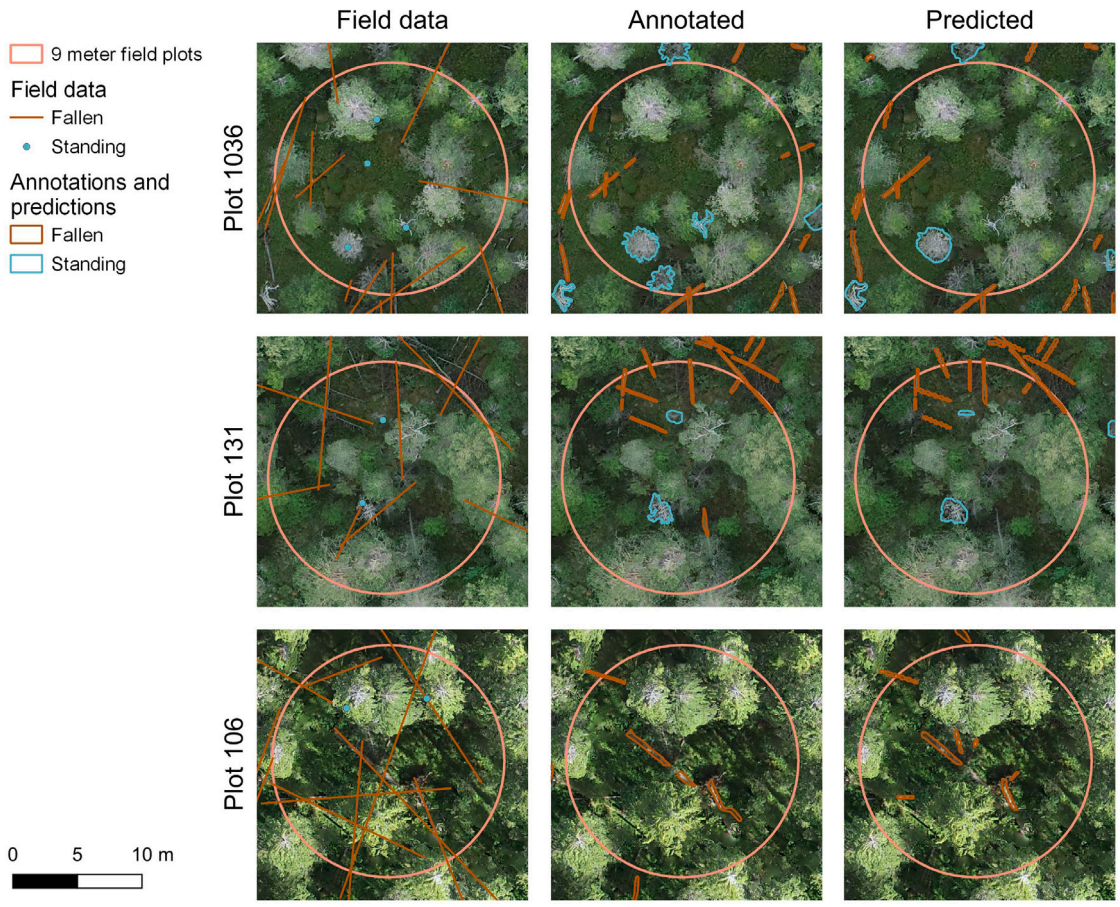

Fig. 9. Comparisons between field data, annotations and predictions from three different field plots.

due to their small size, might be even removed from the images during the orthorectification process. Also, many of the field-measured snags were only a couple of meters tall and standing right next to a living tree, making it practically impossible to detect them from above using passive airborne imagery. If not entirely covered by the surrounding living trees, the standing dead trees with multiple remaining branches can be rather reliably discerned from the living canopy. Another challenge is related to segmenting the individual canopies of larger trees. While the pixels belonging to standing deadwood canopies can be detected accurately (e.g., Schiefer et al., 2023), separating the individual trees can sometimes be difficult even for expert annotators as the canopies standing close to each other can blend into each other. Also, some living trees might have their canopy broken or partially leafless, adding an extra layer of interpretation on whether the tree can be considered to be living or dead.

5.2. Viability of instance segmentation models in deadwood detection

Using YOLOv8 for mapping of downed deadwood resulted in good accuracy when compared to the annotated data (Table 7), as most of the visible deadwood was correctly detected. However, similarly to the annotations, validation against field-measured data showed that although the algorithm itself performs well, it is only as good as its input data, i.e., the UAV images and the annotated training data. In the case of downed deadwood, large share of the objects could not be discerned from the UAV imagery. Canopy cover strongly affects the quality and completeness of annotations as well as the mapping of downed deadwood from image data.

In both of our study areas, models trained with local data performed significantly better than the models trained with data only from the other study site. The gap was especially clear for Sudenpesänkangas area, where the mAP50 scores were consistently 0.2 lower for the models trained with Hiidenportti data. For both datasets the best performance was achieved through models trained with combined dataset, which aligns with Chadwick et al. (2024), who also achieved the best results for canopy segmentation with models trained with data from multiple sites. Utilizing reference datasets from different locations typically combines data from different types of cameras, resolutions, and weather conditions. This results in a more thorough description of the variation of the studied canopies for the modeling process, which seems to be necessary when training a model for varying locations and scenarios. The increasing availability of global datasets for forest research, such as the deadtrees.earth dataset (Kattenborn et al.; Mosig et al., 2024) could be used to train models that perform suitably well in different locations.

As the field of artificial intelligence and computer vision is rapidly advancing, there are several viable frameworks and model architectures, apart from ultralytics and YOLOv8, that could be used for deadwood detection and segmentation tasks. For instance, the latest iteration of the YOLO model family is already YOLOv12 (Tian et al., 2025), and the development shows no signs of slowing down. One especially interesting research direction are the several foundation models for computer vision that have been released during the last couple of years, such as Segment Anything (Kirillov et al., 2023), DINOv2 (Oquab et al., 2024), and Grounding DINO (Liu et al., 2024), which can be used for either segmenting all objects in the image, or giving text-based prompts to the models in order to segment only specific targets. For instance, Segment Anything has shown potential for processing remote sensing data, but there is still room for improvement for it to be operationally viable (Osco et al., 2023). Still, validating these models with good-quality field data is essential for successful operational use.

5.3. Limitations and other approaches

Intuitively, and as our results also indicate, one of the key limitations of image data is its inability in capturing the objects occluded by the canopy. Here, the setup in which the UAV imagery is collected has a significant effect. For instance, the overlap rate between individual UAV images affects how well the resulting orthomosaic or photogrammetric point cloud can penetrate the upper canopy layer. With high overlap rate, canopy penetration is typically better, and a greater share of the forest floor is captured in the image mosaic (Liang et al., 2022). However, in boreal forests with dense canopy, even high overlap rates do not guarantee sufficient visibility below the canopy. In this study, we used relatively high front overlap and side overlap in both of our study areas, resulting in consistent orthomosaics with sufficient spatial resolution at all sites. Having consistent, good quality image data is important for the trustworthiness of the results, especially when designing a methodology which is intended to be applied in multiple different areas and flight campaigns.

The issue of canopy occlusion could also be overcome with alternative remote sensing data. In addition to image-based data, there are other solutions that could improve deadwood mapping. For example, several studies have utilized airborne LiDAR data for fallen deadwood mapping as it can penetrate the canopy and thus detect even some of the fallen trunks directly under the living canopy. The methods have proven to capture the largest and thus ecologically most significant trunks with a rather high accuracy Heinaro et al., 2021). However, acquiring LiDAR data with a high point density ($\geq$15 points/m^2) is still expensive. Especially, this holds for small areas where the full efficiency of plane-operated scanning is not reached. Moreover, while the number of fallen trees that are can be detected with very high-resolution LiDAR data (such as UAV LiDAR), these data might require more advanced analysis methods compared to processing lower resolution point clouds (Heinaro et al., 2023b). Nevertheless, combining results acquired with different close-range remote sensing techniques (e.g., UAV LiDAR and optical data) might improve the results, as their strengths complement each other. Another possible method to see under the canopy would be to generate below-canopy surface model from photogrammetric point clouds (e.g., Thiel et al., 2020) and then detect the deadwood from it with suitable methods. However, the type (evergreen or deciduous) and density of upper canopy and the amount of undergrowth play a major role with this kind of approaches.

Even with the known challenges of aerial optical imagery, namely the fallen deadwood being shadowed and obscured by the living canopy, we consider efficient use of UAVs to improve the state of deadwood data collection, and eventually, a potential means for collecting robust stand-level deadwood estimates. With the increase in the production of large-scale UAV datasets, such as (Kelluu Ltd. et al., 2024), a complete coverage of Koli National Park collected using autonomous blimps, approaches that can efficiently and accurately process large very high-resolution datasets are essential to efficiently utilize the collected data. Although the mapping accuracy of the suggested UAV-based method is not at the level of field inventories, it is able to detect the presence of large dead trees, both standing and fallen. Further studies should address more closely the relationship between visible downed deadwood and canopy cover. Likely, detecting similar amount of deadwood from images in sparse and dense canopies would indicate a larger amount of deadwood in the latter. These type of approaches could help in building robust image-based estimates of deadwood abundance. In method development, it is important to keep in mind that the image-based approaches should be tested against broad field-measured datasets with precise deadwood locations, instead of only validating the methods with object detection metrics and data annotated from images.

6. Conclusions

In this work, we studied the viability of UAV images as a resource to improve the small-scale mapping of deadwood in boreal forests. We assessed how well a current state-of-the-art instance segmentation method YOLOv8 performs in deadwood detection and segmentation from UAV images and how does canopy cover percentage affect the quality and trustworthiness of the detections. We also mixed training data from two origins and examined how does the spatial origin of the training data affect the methods' performance.

The instance segmentation methods were able to detect most of the visible deadwood from the UAV images at similar rate as our experts did. Still, especially the total amount of fallen deadwood was significantly underestimated. The dense canopy made the fallen trunks similarly hard to detect both for the experts and the model. Looking at the spatial origin of the training data, the models trained with data from several locations outperformed the models that were trained with data only from a single location.

Based on our results, current image-based UAV mapping methods cannot provide forest inventory applications with unbiased data concerning, e.g., deadwood volumes. According to our results, image-based methods tend to underestimate the amount of deadwood, and the bias is strongly linked with canopy cover percentage. Still, the methods have high potential to be enhanced. Especially for downed deadwood, focusing further research on the statistical dependencies between canopy cover percentage, visible deadwood, and field-measured deadwood would likely enhance the overall reliability of image-based deadwood mapping. Here, the effect of canopy cover should be quantified to control the bias caused from the occluded deadwood trunks. The largest dead trees can be mapped rather reliably already with present techniques. This means that a significant share of total deadwood volumes, as well as the ecological quality it represents can be detected already with existing methods.

CRediT authorship contribution statement

Janne Mäyrä: Writing – original draft, Software, Methodology, Investigation, Data curation, Conceptualization. **Topi Tanhuanpää:** Conceptualization, Writing – original draft, Investigation. **Anton Kuzmin:** Writing – original draft, Resources, Data curation. **Einari Heinaro:** Writing – original draft, Data curation. **Timo Kumpula:** Writing – original draft, Supervision, Funding acquisition. **Petteri Vihervaara:** Writing – original draft, Supervision, Funding acquisition.

Funding

This study was supported by Strategic Research Council, Finland [project number 312559]; Research Council of Finland [project numbers 347862, 357475]; Finnish Research Infrastructure Committee [project number 345733]; Ministry of the Environment, Finland [VN/5082/2020]; HORIZON EUROPE Research and innovation programme [grant agreement no. 101134954]; LIFE financial instrument of the European Union [LIFE17/NAT/FI/000181]; Doctoral Program in Sustainable Use of Renewable Natural Resources [AGFOREE]; and Interreg Aurora [project number 20366456].

Declaration of competing interest

The authors declare that they have no known competing financial interests or personal relationships that could have appeared to influence the work reported in this paper.

Acknowledgments

The authors would like to thank Max Stranden, Gust Noens and Taneli Vuornos for participating in the annotation process of the deadwood data from UAV imagery. Also, the authors wish to acknowledge CSC — IT Center for Science, Finland, for computational resources.

Data availability

The research codes are shared on GitHub, and the trained model checkpoints are shared on Hugging Face platform.

References

Akyon, F.C., Altinuc, S.O., Temizel, A., 2022. Slicing aided hyper inference and fine-tuning for small object detection. arXiv:2202.06934.

Biewald, L., 2020. Experiment tracking with weights and biases.

Blanchard, S.D., Jakubowski, M.K., Kelly, M., 2011. Object-based image analysis of downed logs in disturbed forested landscapes using lidar. Remote. Sens. 3, 2420–2439. http://dx.doi.org/10.3390/rs3112420.

Bochkovskiy, A., Wang, C.Y., Liao, H.Y.M., 2020. YOLOv4: Optimal speed and accuracy of object detection. http://dx.doi.org/10.48550/arXiv.2004.10934, arXiv:2004.10934.

Chadwick, A.J., Coops, N.C., Bater, C.W., Martens, L.A., White, B., 2022. Species classification of automatically delineated regenerating conifer crowns using RGB and Near-Infrared UAV Imagery. IEEE Geosci. Remote. Sens. Lett. 19, 1–5. http://dx.doi.org/10.1109/LGRS.2021.3123552.

Chadwick, A.J., Coops, N.C., Bater, C.W., Martens, L.A., White, B., 2024. Transferability of a Mask R–CNN model for the delineation and classification of two species of regenerating tree crowns to untrained sites. Sci. Remote. Sens. 9, 100109. http://dx.doi.org/10.1016/j.srs.2023.100109.

Chadwick, A.J., Goodbody, T.R.H., Coops, N.C., Hervieux, A., Bater, C.W., Martens, L.A., White, B., Röeser, D., 2020. Automatic delineation and height measurement of regenerating conifer crowns under Leaf-Off conditions using UAV imagery. Remote. Sens. 12 (4104), http://dx.doi.org/10.3390/rs12244104.

de Carvalho, O.L.F.A., O.L.F.A., de Carvalho, de Albuquerque, A.O., de Bem, P.P., Silva, C.R., Ferreira, P.H.G., de Moura, R.A.T., Guimarães, R.F., Borges, D.L., 2021. Instance segmentation for large, multi-channel remote sensing imagery using mask-RCNN and a mosaicking approach. Remote. Sens. 13, 1–24. http://dx.doi.org/10.3390/rs13010039.

Gibb, H., Ball, J.P., Johansson, T., Atlegrim, O., Hjältén, J., Danell, K., 2005. Effects of management on coarse woody debris volume and composition in boreal forests in northern Sweden. Scand. J. For. Res. 20, 213–222. http://dx.doi.org/10.1080/02827580510008392.

Guo, Q., Kelly, M., Gong, P., Liu, D., 2007. An object-based classification approach in mapping tree mortality using high spatial resolution imagery. GIScience Remote. Sens. 44, 24–47. http://dx.doi.org/10.2747/1548-1603.44.1.24.

Hao, Z., Lin, L., Post, C.J., Mikhailova, E.A., Li, M., Chen, Y., Yu, K., Liu, J., 2021. Automated tree-crown and height detection in a young forest plantation using mask region-based convolutional neural network (Mask R-CNN). ISPRS J. Photogramm. Remote Sens. 178, 112–123. http://dx.doi.org/10.1016/j.isprsjprs.2021.06.003.

He, K., Gkioxari, G., Dollár, P., Girshick, R., 2020. Mask R-CNN. IEEE Trans. Pattern Anal. Mach. Intell. 42, 386–397. http://dx.doi.org/10.1109/TPAMI.2018.2844175, arXiv:1703.06870.

Heinaro, E., Tanhuanpää, T., Kukko, A., Hakala, T., Holopainen, M., 2023a. Comparing field measurements and annotations as training data for UAV-based detection of standing dead trees in coniferous forest. Int. J. Remote Sens. 44, 5375–5396. http://dx.doi.org/10.1080/01431161.2023.2248561.

Heinaro, E., Tanhuanpää, T., Vastaranta, M., Yrttimaa, T., Kukko, A., Hakala, T., Mattsson, T., Holopainen, M., 2023b. Evaluating factors impacting fallen tree detection from airborne laser scanning point clouds. Remote. Sens. 15 (382), http://dx.doi.org/10.3390/rs15020382.

Heinaro, E., Tanhuanpää, T., Yrttimaa, T., Holopainen, M., Vastaranta, M., 2021. Airborne laser scanning reveals large tree trunks on forest floor. Forest Ecol. Manag. 491, 119225. http://dx.doi.org/10.1016/j.foreco.2021.119225.

Hu, G., Wang, T., Wan, M., Bao, W., Zeng, W., 2022. UAV remote sensing monitoring of pine forest diseases based on improved Mask R-CNN. Int. J. Remote Sens. 43, 1274–1305. http://dx.doi.org/10.1080/01431161.2022.2032455.

Inoue, T., Nagai, S., Yamashita, S., Fadaei, H., Ishii, R., Okabe, K., Taki, H., Honda, Y., Kajiwara, K., Suzuki, R., 2014. Unmanned aerial survey of fallen trees in a deciduous broadleaved forest in eastern Japan. PLoS One 9, e109881. http://dx.doi.org/10.1371/journal.pone.0109881.

Jiang, S., Yao, W., Heurich, M., 2019. Dead wood detection based on semantic segmentation of VHR aerial CIR imagery using optimized FCN-Densenet. In: International Archives of the Photogrammetry, Remote Sensing and Spatial Information Sciences - ISPRS Archives. pp. 127–133. http://dx.doi.org/10.5194/isprs-archives-XLII-2-W16-127-2019.

Jocher, G., Chaurasia, A., Qiu, J., 2023. YOLO by ultralytics.

Jocher, G., Stoken, A., Chaurasia, A., Borovec, J., NanoCode012, TaoXie, Kwon, Y, Michael, K., Changyu, L., Fang, J., Laughing, V.A., tkianai, yxNONG, Skalski, P., Hogan, A., Nadar, J., imyhxy, Mammana, AlexWang1900, L., Fati, C., Montes, D., Hajek, J., Diaconu, L., Minh, M.T., Marc, albinxavi, fatih, oleg, 743wang-haoyang0106, 2021. Ultralytics/yolov5: V6.0 - YOLOv5n 'nano' models, roboflow integration, TensorFlow export, OpenCV DNN support. Zenodo http://dx.doi.org/10.5281/zenodo.5563715.

Jonsson, B.G., Ekström, M., Esseen, P.A., Grafström, A., Ståhl, B., 2016. Dead wood availability in managed Swedish forests - Policy outcomes and implications for biodiversity. Forest Ecol. Manag. 376, 174–182. http://dx.doi.org/10.1016/j.foreco.2016.06.017.

Junttila, S., Blomqvist, M., Laukkanen, V., Heinaro, E., Polvivaara, A., O'Sullivan, H., Yrttimaa, T., Vastaranta, M., Peltola, H., 2024. Significant increase in forest canopy mortality in boreal forests in Southeast Finland. Forest Ecol. Manag. 565, 122020. http://dx.doi.org/10.1016/j.foreco.2024.122020.

Juutinen, A., Mönkkönen, M., Sippola, A.L., 2006. Cost-efficiency of decaying wood as a surrogate for overall species richness in boreal forests. Conserv. Biol. 20, 74–84. http://dx.doi.org/10.1111/j.1523-1739.2005.00306.x.

Kattenborn, T., Eichel, J., Fassnacht, F.E., 2019a. Convolutional Neural Networks enable efficient, accurate and fine-grained segmentation of plant species and communities from high-resolution UAV imagery. Sci. Rep. 9, 1–9. http://dx.doi.org/10.1038/s41598-019-53797-9.

Kattenborn, T., Leitloff, J., Schiefer, F., Hinz, S., 2021. Review on Convolutional Neural Networks (CNN) in vegetation remote sensing. ISPRS J. Photogramm. Remote Sens. 173, 24–49. http://dx.doi.org/10.1016/j.isprsjprs.2020.12.010.

Kattenborn, T., Lopatin, J., Förster, M., Braun, A.C., Fassnacht, F.E., 2019b. UAV data as alternative to field sampling to map woody invasive species based on combined Sentinel-1 and Sentinel-2 data. Remote Sens. Environ. 227, 61–73. http://dx.doi.org/10.1016/j.rse.2019.03.025.

Kattenborn, T., Mosig, C., Pratima, K., Frey, J., Perez-Priego, F., Cheng, Y., Potts, A., Jehle, J., Mälicke, M., Mahecha, M., Deadtrees.Earth - an Open, Dynamic Database for Accessing, Contributing, Analyzing, and Visualizing Remote Sensing-Based Tree Mortality Data. Technical Report EGU24-15502, http://dx.doi.org/10.5194/egusphere-egu24-15502, Copernicus Meetings.

Kelluu Ltd., Hietala, Janne, Jormakka, Jiri, Honkavaara, Eija, Koivumäki, Niko, de Oliveira, Raquel Alves, Lyytikäinen-Saarenmaa, Päivi, Tuviala, Johanna, Maanmittauslaitos, et al., 2024. Koli kelluu airship spring 2023. https://doi.org/10.23729/a6e8e2ef-0b72-411c-b011-ceae2d956f3a.

Kirillov, A., Mintun, E., Ravi, N., Mao, H., Rolland, C., Gustafson, L., Xiao, T., Whitehead, S., Berg, A.C., Lo, W.Y., Dollár, P., Girshick, R., 2023. Segment anything. arXiv:2304.02643.

Kuzmin, A., Korhonen, L., Kivinen, S., Hurskainen, P., Korpelainen, P., Tanhuanpää, T., Maltamo, M., Vihervaara, P., Kumpula, T., 2021. Detection of european aspen (populus tremula L.) based on an unmanned aerial vehicle approach in boreal forests. Remote. Sens. 13 (1723), http://dx.doi.org/10.3390/rs13091723.

Laasasenaho, J., 1975. Runkopuun saannon riippuvuus kannon korkeudesta ja latvan katkaisuläpimitasta. Metsäntutkimuslaitos.

Lassauce, A., Paillet, Y., Jactel, H., Bouget, C., 2011. Deadwood as a surrogate for forest biodiversity: Meta-analysis of correlations between deadwood volume and species richness of saproxylic organisms. Ecol. Indic. 11, 1027–1039. http://dx.doi.org/10.1016/j.ecolind.2011.02.004.

Liang, X., Kukko, A., Balenović, I., Saarinen, N., Junttila, S., Kankare, V., Holopainen, M., Mokroš, P., Kaartinen, H., Jurjević, L., Honkavaara, E., Näsi, R., Liu, J., Hollaus, M., Tian, J., Yu, X., Pan, J., Cai, S., Virtanen, J.P., Wang, Y., Hyyppä, J., 2022. Close-range remote sensing of forests: The state of the art, challenges, and opportunities for systems and data acquisitions. IEEE Geosci. Remote. Sens. Mag. 10, 32–71. http://dx.doi.org/10.1109/MGRS.2022.3168135.

Lin, T.Y., Maire, M., Belongie, S., Hays, J., Perona, P., Ramanan, D., Dollár, P., Zitnick, C.L., 2014. Microsoft COCO: Common Objects in Context. In: Lecture Notes in Computer Science (Including Subseries Lecture Notes in Artificial Intelligence and Lecture Notes in Bioinformatics), pp. 740–755. http://dx.doi.org/10.1007/978-3-319-10602-1_48, arXiv:1405.0312.

Liu, S., Zeng, Z., Ren, T., Li, F., Zhang, H., Yang, J., Jiang, Q., Li, C., Yang, J., Su, H., Zhu, J., Zhang, L., 2024. Grounding DINO: Marrying DINO with grounded pre-training for open-set object detection. http://dx.doi.org/10.48550/arXiv.2303.05499, arXiv:2303.05499.

Mäyrä, J., Keski-Saari, S., Tanhuanpää, T., Hurskainen, P., Kullberg, P., Poikolainen, L., Viinikka, A., Tuominen, S., Kumpula, T., Vihervaara, P., 2021. Tree species classification from airborne hyperspectral and LiDAR data using 3D convolutional neural networks. Remote Sens. Environ. 256, 112322. http://dx.doi.org/10.1016/j.rse.2021.112322.

Mosig, C., Vajna-Jehle, J., Mahecha, M.D., Cheng, Y., Hartmann, H., Montero, D., Junttila, S., Horion, S., Schwenke, M.B., Adu-Bredu, S., Al-Halbouni, D., Allen, M., Altman, J., Angiolini, C., Astrup, R., Barrasso, C., Bartholomeus, H., Brede, B., Buras, A., Carrieri, E., Chirici, G., Cloutier, M., Cushman, K.C., Dalling, J.W., Dempewolf, J., Denter, M., Ecke, S., Eichel, J., Eltner, A., Fabi, M., Fassnacht, F., Feirreira, M.P., Frey, J., Frick, A., Ganz, S., Garbarino, M., García, M., Gassilloud, M., Ghasemi, M., Giannetti, F., Gonzalez, R., Gosper, C., Greinwald, K., Grieve, S., Gutierrez, J.A., Göritz, A., Hajek, P., Hedding, D., Hempel, J., Hernández, M., Heurich, M., Honkavaara, E., Jucker, T., Kalwij, J.M., Khatri-Chhetri, P., Klemmt, H.J., Koivumäki, N., Korznikov, K., Kruse, S., Krüger, R., Laliberté, E., Langan, L., Latifi, H., Lehmann, J., Li, L., Lines, E., Lopatin, J., Lucieer, A., Ludwig, M., Ludwig, A., Lyytikäinen-Saarenmaa, P., Ma, Q., Marino, G., Maroschek, M., Meloni, F., Menzel, A., Meyer, H., Miraki, M., Moreno-Fernández, D., Muller-Landau, H.C., Mälicke, M., Möhring, J., Müllerova, J., Neumeier, P., Näsi, R., Oppgenoorth, L., Palmer, M., Paul, T., Potts, A., Prober, S., Puliti, S., Pérez-Priego, C., Rossi, C., Ruehr, N.K., Ruiz-Benito, C.M., Scherer-Lorenzen, F.,

Schladebach, J., Schmehl, M.T., Schwarz, S., Seidl, R., Shafeian, E., de Simone, L., Sohrabi, H., Sotomayor, L., Sparrow, B., Steer, B.S.C., Stenson, M., Stöckigt, B., Su, Y., Suomalainen, J., Torresani, M., Umlauft, J., Vargas-Ramírez, N., Volpi, M., Vásquez, V., Weinstein, B., Ximena, T.C., Zdunic, K., Zielewska-Büttner, K., de Oliveira, R.A., van Wagtendonk, L., von Dosky, V., Kattenborn, T., 2024. Dead-trees.earth - An open-access and interactive database for centimeter-scale aerial imagery to uncover global tree mortality dynamics. http://dx.doi.org/10.1101/2024.10.18.619094.

Mücke, W., Deák, B., Schroiff, A., Hollaus, M., Pfeifer, N., 2013. Detection of fallen trees in forested areas using small footprint airborne laser scanning data. Can. J. Remote Sens. 39, S32–S40. http://dx.doi.org/10.5589/m13-013.

Næsset, E., 2002. Predicting forest stand characteristics with airborne scanning laser using a practical two-stage procedure and field data. Remote Sens. Environ. 80, 88–99. http://dx.doi.org/10.1016/S0034-4257(01)00290-5.

Oquab, M., Darcet, T., Moutakanni, T., Vo, H., Szafraniec, M., Khalidov, V., Fernandez, P., Haziza, D., Massa, F., El-Nouby, A., Assran, M., Ballas, N., Galuba, W., Howes, R., Huang, P.Y., Li, S.W., Misra, I., Rabbat, M., Sharma, V., Synnaeve, G., Xu, H., Jegou, H., Mairal, J., Labatut, P., Joulin, A., Bojanowski, P., 2024. DINOv2: Learning robust visual features without supervision. http://dx.doi.org/10.48550/arXiv.2304.07193, arXiv:2304.07193.

Osco, L.P., Wu, Q., de Lemos, E.L., Gonçalves, W.N., Ramos, A.P.M., Li, J., Marcato, J., 2023. The segment anything model (SAM) for remote sensing applications: from zero to one shot. Int. J. Appl. Earth Obs. Geoinf. 124, 103540. http://dx.doi.org/10.1016/j.jag.2023.103540.

Packalén, P., Maltamo, M., 2007. The k-MSN method for the prediction of species-specific stand attributes using airborne laser scanning and aerial photographs. Remote Sens. Environ. 109, 328–341. http://dx.doi.org/10.1016/j.rse.2007.01.005.

Pasher, J., King, D.J., 2009. Mapping dead wood distribution in a temperate hardwood forest using high resolution airborne imagery. Forest Ecol. Manag. 258, 1536–1548. http://dx.doi.org/10.1016/j.foreco.2009.07.009.

Pirotti, F., Travaglini, D., Giannetti, F., Kutchartt, E., Bottalico, F., Chirici, G., 2016. Kernel feature cross-correlation for unsupervised quantification of damage from windthrow in forests. In: International Archives of the Photogrammetry, Remote Sensing and Spatial Information Sciences - ISPRS Archives. pp. 17–22. http://dx.doi.org/10.5194/isprsarchives-XLI-B7-17-2016.

Polewski, P., Shelton, J., Yao, W., Heurich, M., 2021. Instance segmentation of fallen trees in aerial color infrared imagery using active multi-contour evolution with fully convolutional network-based intensity priors. ISPRS J. Photogramm. Remote Sens. 178, 297–313. http://dx.doi.org/10.1016/j.isprsjprs.2021.06.016, arXiv:2105.01998.

Polewski, P., Yao, W., Heurich, M., Krzystek, P., Stilla, U., 2015. Detection of fallen trees in ALS point clouds using a Normalized Cut approach trained by simulation. ISPRS J. Photogramm. Remote Sens. 105, 252–271. http://dx.doi.org/10.1016/j.isprsjprs.2015.01.010.

Puletti, N., Canullo, R., Mattioli, W., Gawryś, R., Corona, P., Czerepko, J., 2019. A dataset of forest volume deadwood estimates for Europe. Ann. For. Sci. 76, 1–8. http://dx.doi.org/10.1007/s13595-019-0832-0.

Redmon, J., Divvala, S., Girshick, R., Farhadi, A., 2016. You only look once: unified, real-time object detection. arXiv:1506.02640.

Redmon, J., Farhadi, A., 2016. YOLO9000: Better, faster, stronger. http://dx.doi.org/10.48550/arXiv.1612.08242, arXiv:1612.08242.

Redmon, J., Farhadi, A., 2018. YOLOv3: an incremental improvement. http://dx.doi.org/10.48550/arXiv.1804.02767, arXiv:1804.02767.

Ren, S., He, K., Girshick, R., Sun, J., 2017. Faster R-CNN: towards real-time object detection with region proposal networks. IEEE Trans. Pattern Anal. Mach. Intell. 39, 1137–1149. http://dx.doi.org/10.1109/TPAMI.2016.2577031, arXiv:1506.01497.

Ronneberger, O., Fischer, P., Brox, T., 2015. U-net: convolutional networks for biomedical image segmentation. In: Lecture Notes in Computer Science (Including Subseries Lecture Notes in Artificial Intelligence and Lecture Notes in Bioinformatics). Springer Verlag, pp. 234–241. http://dx.doi.org/10.1007/978-3-319-24574-4_28, arXiv:1505.04597.

Schiefer, F., Kattenborn, T., Frick, A., Frey, J., Schall, P., Koch, B., Schmidtlein, S., 2020. Mapping forest tree species in high resolution UAV-based RGB-imagery by means of convolutional neural networks. ISPRS J. Photogramm. Remote Sens. 170, 205–215. http://dx.doi.org/10.1016/j.isprsjprs.2020.10.015.

Schiefer, F., Schmidtlein, S., Frick, A., Frey, J., Klinke, R., Zielewska-Büttner, S., Uhl, A., Kattenborn, T., 2023. UAV-based reference data for the prediction of fractional cover of standing deadwood from Sentinel time series. ISPRS Open J. Photogramm. Remote. Sens. 8, 100034. http://dx.doi.org/10.1016/j.ophoto.2023.100034.

Schwarz, S., Werner, C., Fassnacht, F.E., Ruehr, N.K., 2024. Forest canopy mortality during the 2018–2020 summer drought years in Central Europe: The application of a deep learning approach on aerial images across Luxembourg. For.: Int. J. For. Res. 97, 376–387. http://dx.doi.org/10.1093/forestry/cpad049.

Stokland, J.N., Siitonen, J., Jonsson, B.G., 2012. Biodiversity in Dead Wood. Cambridge University Press.

Sylvain, J.D., Drolet, G., Brown, N., 2019. Mapping dead forest cover using a deep convolutional neural network and digital aerial photography. ISPRS J. Photogramm. Remote Sens. 156, 14–26. http://dx.doi.org/10.1016/j.isprsjprs.2019.07.010.

Thiel, C., Mueller, M.M., Epple, L., Thau, C., Hese, S., Voltersen, M., Henkel, A., 2020. Uas imagery-based mapping of coarse wood debris in a natural deciduous forest in central Germany (Hainich National Park). Remote. Sens. 12, 1–24. http://dx.doi.org/10.3390/rs12203293.

Tian, Y., Ye, Q., Doermann, D., 2025. Yolov12: Attention-centric real-time object detectors. arXiv preprint arXiv:2502.12524.

Tuominen, S., Pitkänen, J., Balazs, A., Korhonen, K.T., Hyvönen, P., Muinonen, E., 2014. NFI plots as complementary reference data in forest inventory based on airborne laser scanning and aerial photography in Finland. Silva Fenn. 48, http://dx.doi.org/10.14214/sf.983.

Viinikka, A., Hurskainen, P., Keski-Saari, S., Kivinen, S., Tanhuanpää, T., Mäyrä, J., Poikolainen, L., Vihervaara, P., Kumpula, T., 2020. Detecting European Aspen (populus tremula L.) in boreal forests using airborne hyperspectral and Airborne Laser Scanning Data. Remote. Sens. 12 (2610), http://dx.doi.org/10.3390/rs12162610.

Yuan, Q., Shen, H., Li, T., Li, Z., Li, S., Jiang, Y., Xu, H., Tan, W., Yang, Q., Wang, J., Gao, J., Zhang, L., 2020. Deep learning in environmental remote sensing: Achievements and challenges. Remote Sens. Environ. 241, 111716. http://dx.doi.org/10.1016/j.rse.2020.111716.

Zhang, C., Zhou, J., Wang, H., Tan, T., Cui, M., Huang, Z., Wang, P., Zhang, L., 2022. Multi-species individual tree segmentation and identification based on improved mask R-CNN and UAV imagery in mixed forests. Remote. Sens. 14 (874), http://dx.doi.org/10.3390/rs14040874.